Pascual-Cebrian et al. 2013. High resolution and true colour grinding tomography of rudist bivalves, exemplified with the taxonomic revision of *Mathesia darderi* (Astre). *Caribbean Journal of Earth Science*, volume **45**, 35-46.
 Available online 12th March 2013.

High resolution and true colour grinding tomography of rudist bivalves, exemplified with the taxonomic revision of *Mathesia darderi* (Astre)

ENRIC PASCUAL-CEBRIAN, DOMINIK K. HENNHÖFER AND STEFAN GÖTZ[+]

Institute for Earth Sciences, Heidelberg University, Im Neuenheimer Feld 234, 69120 Heidelberg, Germany. e-mail: enric.pascual@geow.uni-heidelberg.de. [+]deceased.

ABSTRACT. The tomography of fossils is based on the production of numerous sequential high-resolution pictures (tomograms) that form the base for a later three-dimensional evaluation. X-ray computed tomography proved to be the most successful method in tomography but has its limitations with samples of low-density differences. Here, we describe a technique using grinding tomography that can produce high resolution, true colour images in limestone samples. The method is based on automatic serial grinding and serial scanning. The working process starts with embedding the samples in a mould with epoxide resin. The hardened block is then polished with a precision surface-grinding machine. After each polishing step, the surfaces are scanned with a modified flatbed scanner fitted with a water bath and a system for aligning the tomograms. The maximum resolution of this method is equivalent to a voxel size of around 10 µm^3. The productivity is determined by the resolutions, both vertical and horizontal, and the block size; to increase the efficiency multiple specimens can be embedded in the same block. The method has potential for studies on taxonomy, ontogeny, population dynamics and shell mineralogy. To exemplify the potential of this method in taxonomy we have revised the myocardinal apparatus of *Mathesia darderi* (Astre).

Key words: tomography, three-dimensional, rudists, reconstruction, grinding, *Petalodontia*, *Mathesia*.

1. INTRODUCTION

Rudist bivalves are usually preserved as three-dimensional fossils in limestone matrix; therefore the isolation of the specimens from the host-rock is usually complicated, time consuming and only reveals the external characters. Serial slicing is a valuable tool for obtaining information about internal structures of organisms. This technique has proven to be useful in the evaluation of intraspecific variations in rudist specimens, as for example shown by Pons and Vicens (1988), Reali (1992), Vicens (1994), Simonpietri and Philip (2000), among others. The study of spatio-temporal variations, such as ontogeny and population dynamics, the quantification of the shell mineralogy and the study of spatial distribution of complex internal features require tomographic methods. Tomography provides information in cross-sections throughout the specimens and offers an adequate number of tomograms that allows visualisation in three dimensions and measuring lengths, areas, angles and volumes. Tomographic techniques can be divided into preservative and non-preservative techniques. A full review is provided by Sutton (2008). Preservative techniques use waves that detect physical variations, among them, X-ray tomography proved to be the most successful method in fossils (e.g., Molineux et al., 2007). Destructive techniques are based on the physical exposure of the surfaces; those are serial grinding and serial sawing. In this publication we describe the advantages of different tomographic techniques for rudist bivalves and finally a tomographic technique based on grinding tomography that is also suitable for big fossils. This technique has been exemplified with the taxonomic description of a dense bouquet of *Mathesia darderi* (Astre). This bouquet was ground in 0.2 mm steps resulting in 420 consecutive tomograms. From these tomograms a single specimen has been isolated and reconstructed using isosurface rendering with the biomedical software OsiriX (Rosset et al., 2004) and Meshlab V1.3.0a software (a tool developed with the support of the 3D-CoForm project); the reconstruction of the right valve shows the external characters, the reconstruction of the left valve shows the arrangement of the myocardinal apparatus. Moreover, other applications for rudist bivalves, such as the study of the shell mineralogy, ontogeny and population dynamics are described.

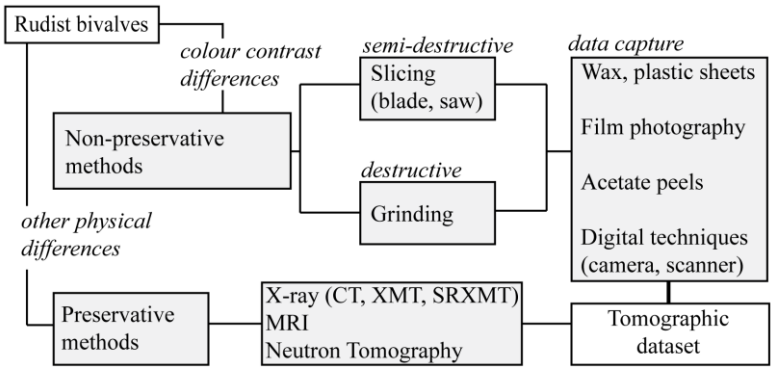

Figure 1. The most common tomographic methods used in palaeontology, divided in preservative and non-preservative methods. The method presented here is based on grinding and scanning. Magnetic resonance imaging (MRI), computed tomography (CT), X-ray microtomography (XMT) and synchrotron radiation X-ray microscope (SRXMT).

1.1 Non-destructive methods.

Preservative or non-destructive methods (**Figure 1**) are able to illustrate physical differences of a material. Neutron tomography (NT) provides a spatial resolution between 0.1 mm and 0.27 mm detecting differences in the concentration of some light elements. It has been successfully used in creating images of vertebrates (Schwarz et al., 2005) and is suitable for preserved organic matter in fossils. The potential of NT in rudist bivalves is not known because it is necessary to determine which sediments and compositions of the shell offer optimal contrast in NT. Magnetic resonance imaging (MRI) produces images at resolutions up to 50 µm and has been used in invertebrates, vertebrates and plants (Mietchen et al., 2008). This tomographic technique has not yet been used on rudist bivalves, although it may be useful for rudists that preserve the original porosity of the internal cavities and for shells that are rich in organic components. Scanners based on X-rays measure the attenuation coefficient of a material, presenting X-ray attenuation maps. These techniques provide detailed measurements in 3-D images with voxel resolutions of less than 5 µm. For example, Dominguez et al. (2002) used CT on a specimen of *Jaekelocarpus oklahomensis* with 0.016 mm of inter-slice spacing. Moreover, the X-ray synchrotron microtomography (SRXTM) offers the opportunity to work with very small features (Tafforeau et al., 2006) such as the buccal apparatus of ammonites (Kruta et al., 2011). This non-destructive technique proved to be very useful for rare and type fossils. The limitations of CT include difficulties in the penetration of X-rays in dense materials and obtaining high-resolution tomograms with low-density differences. This represents a frequent problem in carbonates, when fossils and matrix can have similar or identical densities. In rudist bivalves, X-ray medical computed tomography (CT) shows the general outlines of rudist bivalves with low-density differences (Hughes et al., 2004). Special cases with excellent density differences exist, such as silicified rudist shells in a carbonate matrix. In this case detailed reconstructions of the internal features have been shown at the High-Resolution X-ray Computed Tomography Facility at The University of Texas at Austin (UTCT) (Molineux et al., 2007; Molineux et al., 2010; Scott and Weaver, 2010).

1.2. Destructive methods.

Non-preservative or destructive methods provide tomograms by serial slicing or serial grinding. In serial slicing methods parallel cuts are produced with a saw or a blade exposing several surfaces. In general, saws are used for mineralised fossils and blades for soft fossils. In both techniques the material in between the cuts is preserved. Disadvantages of a data set produced by serial sawing are the low resolution in inter-section space (>1 mm) and its poor cutting precision, resulting in non-parallel and irregular surfaces.

In serial grinding methods, thicknesses of material are abraded from a single planar surface that is captured at each step. The first types of grinding devices were used to polish crystal plates and prisms (e.g. Tutton, 1894). The first machine to grind fossils was constructed by Sollas (1903) to determine the inner structure of vertebrates (Sollas and Sollas, 1914). After these pioneer works, different grinding techniques appeared (e.g., Wright, 1915; Simpson, 1933; Zdanski, 1938; Olsen and Whitmore, 1944; Croft, 1950; Ager, 1965; Sutton et al., 2001). The main disadvantage of grinding is that the sample becomes completely destroyed. Positive aspects are that this technique can be used for broad a range of fossil sizes, producing very accurate and parallel surfaces, with a wide range of resolutions from 10 µm up to several millimetres. Significant studies from the last few years were: Hammer (1999), who used grinding

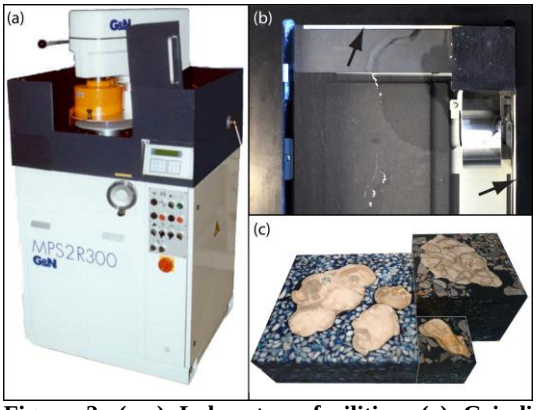

Figure 2. (a-c) Laboratory facilities: (a) Grinding machine G&N MPS 2-R300 (b) Detail of the water quench and the alignment system (black arrows) scanning a small block (5 x 5 cm) (c) The different blocks 5 x 5 cm, 10 x 10 cm and 15 x 15 cm.

tomography in tabulate corals, with a vertical resolution of 100 µm; Siveter et al. (2003) who described the soft parts of an ostracode reconstructed by grinding the specimen at 20 µm intervals; Sutton et al. (2005), who studied Silurian brachiopods with a vertical resolution of 20 µm, and Götz (2007) and Hennhöfer et al. (2012) who both worked on rudist palaeobiology with a vertical resolution of 500 µm and 100 µm, respectively.

1.3. Data capture in destructive methods.

For data capture different methods can be applied: Traces made from wax, plastic sheets, graphic reconstructions and peels (Born, 1883; Sollas and Sollas, 1914; St. Joseph, 1937; Muir-Wood, 1934; Ovcharenko, 1967; Walton, 1928). Today, most of these methods are replaced by digital methods using cameras and scanners. Digital cameras are used for tomogram capturing (e.g., Sutton et al., 2001; Watters and Grotzinger, 2001) because they quickly provide high quality tomograms. However, digital cameras demand constant light conditions and the tomograms cannot be aligned during the capture process. Alignment is carried out manually post-capture with image software. The method presented in this work uses a scanner for data capture. The use of flatbed scanners was introduced by Hammer (1999) to study tabulate corals. The block containing the specimens is aligned to one of the corners of the glass plate of the scanner. This registration system avoids later complicated image alignment processes in the computer. Moreover, scanners offer higher resolutions, and constant light and focusing conditions.

2. TECHNIQUE

The technique described here is based on the abrasion of a consistent thickness of material by a diamond wheel from a planar surface (**Figure 2**). After each grinding cycle the surfaces are digitally captured using a custom built flatbed scanner. The workflow substantially involves three steps: embedding of the samples in a resin block, repeated grinding/polishing and scanning after each polishing step (**Figure 3**).

2.1. Laboratory facilities.

Precision surface grinding machine. The device presented here is a G&N MPS 2-R300 surface precision machine which is used in geosciences for producing thin sections (Figure 3a). A metallic wheel with synthetic diamonds carries out the grinding process. It removes the material by abrasion under water spray conditions. The wheel moves down on the block, which is held on a rotary table by air suction. The abrasion process can be either manual or automatic. The vertical abrasion in the automatic mode can be adjusted between several millimetres and 10 µm, with a precision of 3 µm.

High Resolution Scanner. The method requires a resistant scanner that supports the weight of the blocks and is also able to quickly produce high quality images. We use a custom-built flatbed scanner based on Epson perfection V750 pro (Figure 2, b), with a true physical resolution of 2540 dpi (tested with USAF 1951 test target) and an optical density of 4 (Figure 4). For further improvement, a water bath on the scan area and an adjustment system for the blocks has been mounted to the scanner. The purpose of the water bath is to enhance contrast and resolution, and the liquid avoids reflections of potential scratches in the scanner glass. After testing oils, alcohol and water (purified) as scan liquids, the pictures scanned with water provide better quality images than those scanned in oil. Although alcohol even produces slightly better picture qualities, liquid mixing with water from the grinding machine might decrease the picture quality. Additionally, a drop of washing up liquid is added to the water to decrease surface tension and to enhance the penetration depth of the liquid. The plastic frame also reduces the risk of glass breakage and, consequently, the loss of the scanner. Metallic guides have been installed to the plastic frame to keep the block in the same position in the scan area (**Figure 2b**). Therefore, each tomogram is scanned in the exact same position avoiding later time consuming computer adjustments in the picture stack. Finally, in order to

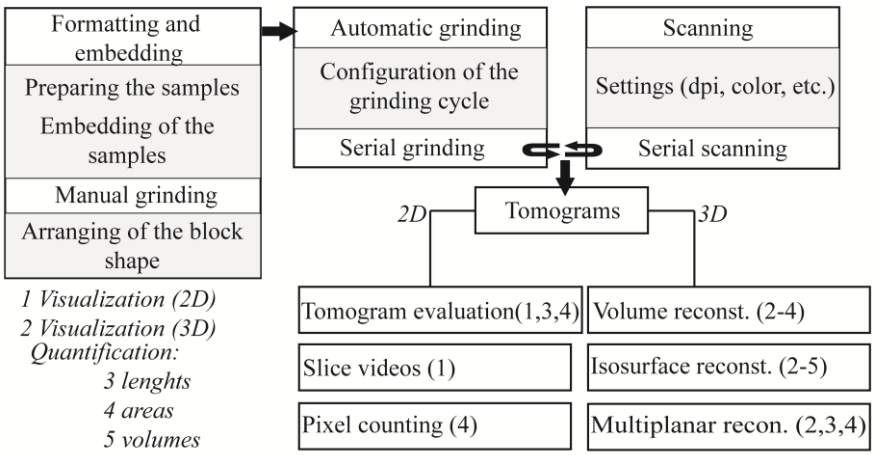

Figure 3. Workflow of the different processes of the method which starts formatting and embedding the samples in resin blocks. Then the block is prepared in the manual mode and finally is stepwise polished and scanned.

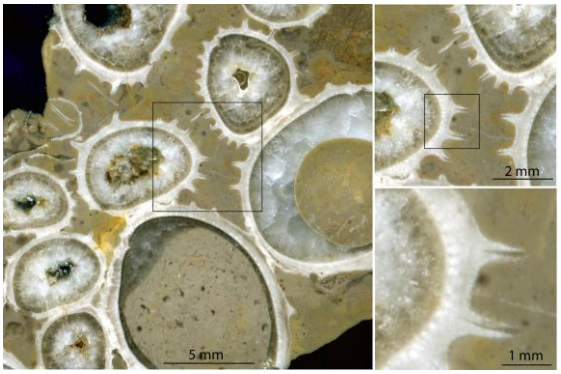

Figure 4. High resolution tomogram of a bouquet of *Mathesia darderi* (2540 dpi). The inner part of the outer calcitic shell layer shows a tubular microstructure.

facilitate the correct position of the sample-block on the scanner and a correct distribution of the distilled water, the scanner is inclined towards the upper right corner.

2.2. Technique description.

Preparing the specimens for grinding. The purpose of sample preparation is to standardise the method according to the demands of the G&N MPS 2 – R300. Therefore the samples are formatted and later embedded with resin in metallic moulds. Due to the destructive nature of the method, any sample should be photographed, measured and duplicated as a plaster cast previous to the process. This is vitally important for rare specimens.

Formatting starts with arranging the size of the samples which have to fit into one of the three metallic moulds: 5 x 5 x 7 cm^3, 10 x 10 x 20 cm^3 and 15 x 15 x 30 cm^3 (**Figure 2c**). The biggest sample that can be processed as a single piece is 15 x 15 x 30 cm^3. The moulds consist of five aluminium plates joined by screws. The embedding process starts with scattering a thin layer of release agent (e.g., Formula Five® Mold Release Wax) on all the metallic surfaces in contact with the resin. In the big moulds this task is essential because the extraction of the block is complicated. The metallic moulds are filled with gravel, epoxide resin, colourant and one to several samples. The lowermost two centimetres of the mould function as a socket for comfortable handling on the machine and scanner and therefore only consist of gravel. In the next step the mould is filled with pigmented epoxide resin. Blue powder pigment is added to the resin to avoid reflections and scanning of inner parts of the block and to increase the contrast between resin and sample. The position of the sample inside the metallic mould determinates the orientation of the cuts and scans throughout the samples.

Epoxide resin. After testing different epoxide resins we decided to use SpeciFix-20 (Struers) due to its high hardness (84 in the Shore D scale) and the short curing time (8 hours) at room temperature. Moreover, before hardening this resin has a low viscosity and is able to fill the pores between gravel and sample and increases the resistance of soft and fragile samples.

Physical behaviour of the block. Even though the epoxide resin used here has good physical characteristics it is still more ductile than the rock samples. Grinding machines are not designed to grind ductile materials. Therefore a high proportion of resin in respect to the rock samples decreases the efficiency of the technique. Mixing gravel and resin increases the rigidity of the block during the grinding process and improves the grinding performance by cleaning the diamond disk from stuck resin. The best results are reached when sample and gravel are of the same lithology, resulting in a more homogeneous mechanical behaviour of the block. In these conditions the finishing of the machine is more precise and the image quality is better.

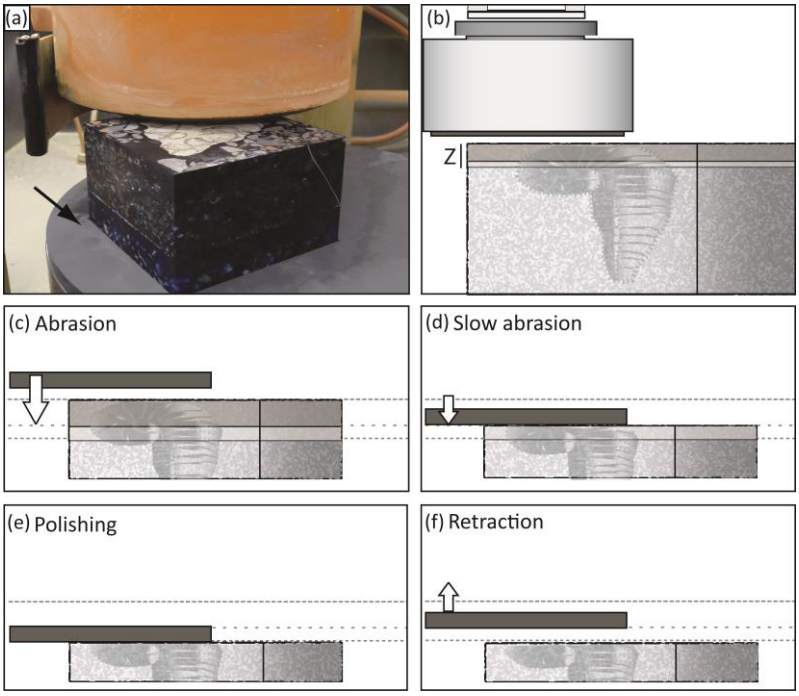

Figure 5. (a) Close-up image of grinder and rotary table with a 10 x 10 cm block. The white arrow represents the sense of rotation of the table; (b) Z is the vertical resolution which is equivalent to the space in between tomograms, the dark grey intervals are ground by fast velocity during the abrasion phase and the light grey intervals are ground by relative slow velocities; (c-f) four phases of one grinding cycle: (c) abrasion; (d) slow abrasion; (e) polishing; (f) retraction.

Reshaping the block for serial grinding. During hardening the resin minimally shrinks such that the adjacent sides of the block do not longer lie at right angles to one another. This lack can lead to imprecise tomographic reconstructions. This problem can be solved by manually reshaping the sides of the block in the GSM grinder before automatic grinding. The aim of the reshaping is to improve the air suction on the rotary table and to achieve a 90° angle that fits perfectly in the alignment unit of the scanner. Finally, the top surface is ground in fast mode until the top most sample appears.

Disk grain sizes. The grain size of the grinding wheel determines the material removal rate and the surface relief. Normally, coarser grain sizes will achieve a higher removal rate, but usually at the expense of high surface quality. Conversely, finer grain sizes achieve better surface qualities, at the expense of reduced material removal. This balance between material removal on one hand and surface quality on the other hand means that many grinding operations need rough grinding followed by finish grinding. Our grinding laboratory provides wheels of different grain sizes: D15, D30, D46 and D91 (from finest to coarsest). Usually we use the disk D91 for reshaping the block, the disk D46 for vertical resolutions greater than 0.3 mm, the disk D30 for vertical resolutions between 300 µm and 30 µm and the disk D15 for vertical resolution between 30 µm and 10 µm.

Automatic serial grinding. The block is placed on a rotary table which is connected to a vacuum pump fixing the block during grinding. During one grinding cycle a specific thickness of material is removed (z), which is equivalent to the distance between two successive tomograms. This value is equal to the vertical resolution (z) of the tomographic data set. Based on our grinding experience with fossils, we use a four phase cycle: Abrasion, slow abrasion, polishing and retraction (**Figure 5c-f**).

The first phase (abrasion) quickly removes the major amount of the thickness. The second phase (slow abrasion) removes the remaining thickness by slow and precise down feed. During the polishing phase the wheel rotates in the same position for 10 – 20 seconds (depending on the requested quality) to minimise the relief of the surface. Finally, the grinder retracts (retraction phase) allowing the removal of the block from the machine.

3. METHOD EFFICIENCY

Methods based on abrasive powder (e.g., Croft, 1950; Ager, 1965) require more time grinding and cleaning the surface than methods based on diamond wheels (Hendry et al., 1963). Both methods can achieve similar accuracies (Sandy, 1989). For example Sutton et al. (2001) used a method based on abrasive powder and needed an average of 6 minutes to grind and interval of 30 µm and one minute to take a photographic picture each

specimen (**Figure 6**, circle). Watters and Grotzinger (2001) used a surface-grinding machine, the interval in between tomograms was 25.4 µm and the surfaces were captured by a digital camera, producing six or seven tomograms per hour (Figure 6, square). The grinding machine described by Hendry et al. (1963) ground a surface of 5 x 4 cm^2 at 10 µm intervals, the surfaces were captured by peels, producing 25 peels per hour (**Figure 6**, hexagon). To measure the efficiency of the method described here we counted the amount of tomograms produced per hour (**Figure 6**) the efficiency in the Heidelberg Tomography Laboratory varies from 4 to 39 tomograms per hour and depends on the vertical resolution (z), the size of the block and the resolution of the images. The size of the specimen and the vertical resolution (z) determines the quantity of tomograms in which the specimens are ground. The resolution of the grinding machine is between 10 µm and several millimetres and determines the downfeed velocity of the grinder. Based on our experience these velocities are between 25 µm/min and 200 µm/min; higher resolutions (z) demand slow velocities (**Figure 6**). The time required for scanning depends on the area and on the image resolution that usually ranges between 600 dpi and 2540 dpi. In rudist pixel size from the scanned image and the distance between tomograms (z) defined by the grinding cycle. The highest resolution that can be achieved equals a voxel size of about 10 × 10 × 10 µm (Scanning: 2540 dpi = 10 µm; Grinding: 10 µm). However, high resolution also induces time consuming grinding and scanning. Therefore both vertical (z) and horizontal resolutions are evaluated individually according to the demands that are required for each sample. To improve efficiency, various samples with similar requirements can be embedded to a single block.

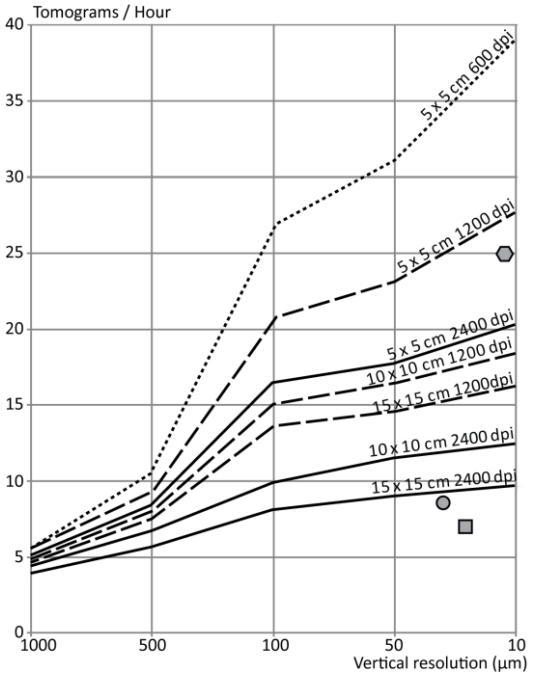

Figure 6. Number of tomograms produced in 1 hour. Vertical resolutions (z), horizontal resolutions: 600 dpi (dotted line), 1200 dpi (dashed line) and 2400 dpi (solid line) and the size of the blocks: 5 x 5 cm, 10 x 10 and 15 x 15 cm. Grinding cycles with vertical resolutions z > 0.5 mm have similar productivities for all the blocks and horizontal resolutions, due to most of the time is consumed grinding. Other methods: Circle (grinding powder and digital photography, Sutton et al., 2001); square (grinding machine and digital photography, Watters and Grotzinger, 2001) and hexagon (grinding machine and peels Hendry et al., 1963).

4. APPLICATIONS

4.1. Ontogeny.

For the observation of different ontogenetic stages in a species it is necessary to create tens of serial sections throughout several specimens, showing different developments of shell ornamentation, myocardinal system and shell microstructures. The grinding tomography method described here allows the study of small features such as the myocardinal system of juvenile bivalves, which cannot be studied in images of CT scanners. For example, Götz (2003) used grinding tomography to divide seven ontogenetic stages in *Hippuritella vasseuri* (Douvillé).

4.2. Mineralogy.

The outer shell layer of rudists is built up of low-magnesium calcite, the inner shell layer of aragonite. The aragonitic shell layer is usually converted to calcite. In this case methods based on X-rays cannot differentiate the shell layers. To this day only physical-optical tomography methods such as grinding tomography can quantify the original volumes of these polymorphs by manually digitalizing the shell layers with image software and quantifying using pixel counting tools or by reconstructing the volumes of the shell layers with 3D image software.

4.3. Population dynamics.

Tomograms through rudist lithosomes can offer detailed information on palaeobiological questions such as reproduction or population dynamics (Götz, 2007). When a population is ground in transverse

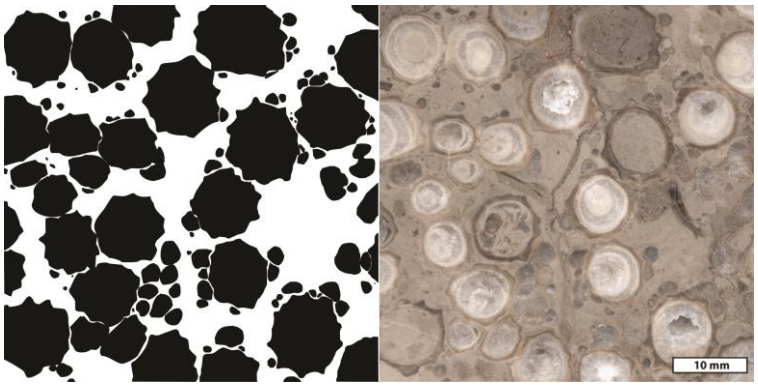

Figure 7. Quantitative analysis in a dense rudist community. The right picture shows an original tomogram from a *Biradiolites mooretownensis* Trechmann bouquet, the left picture shows the area occupied by rudists (coverage) of the same tomogram.

sections, each tomogram represents a specific time interval during growth. Statistical evaluations as well as counting of larvae, adult organisms and spatial relations and developments can give high-resolution insight into fossil communities. Reproductive cycles, area coverage (**Figure 7**), and packing density, settlement of larvae, accommodation space are values that also allow the comparison of different lithosomes in terms of climatic effects and generational overturn (Götz and Stinnesbeck, 2003; Götz, 2005; Götz, 2007; Hennhöfer et al., 2012).

4.4. Systematic palaeontology.

Serial tomograms offer the possibility to visualize the internal features of rudists. However, the orientation of the tomograms is constant and the specimens cannot be inspected from other orientations. To overcome this limitation the tomograms can be reconstructed with 3D image software (e.g., Osirix, 3D Slicer) allowing visualizing and quantifying the specimens in a 3D workspace (e.g., Pascual-Cebrian et al., 2012). To exemplify the potential of this technique a specimen of *Mathesia darderi* (Astre) was described. A monospecific bouquet of *Mathesia darderi* was collected at the Cabo de Ajo headland (Spain) in the Cabo de Ajo section (Baron-Szabo and Fernández-Mendiola, 1997, figure 3 therein, about 270 m). The age of the bearing strata is Early Albian, biostratigraphyally correlated on the basis of benthic foraminifers (Pascal, 1985).

5. GENERIC PLACEMENT OF THE TAXON

The genus *Mathesia* Mainelli belongs to the petalodontid group, an informal sub-grouping in the family Monopleuridae (sensu Masse and Fenerci-Masse, 2009), characterized by having a myophoral plate in the LV. Following the taxonomic reappraisal of Masse and Fenerci-Masse (2010) this genus is represented by one species, *Mathesia darderi* (Astre), incorporating the originally described "*Agria*" *darderi* Astre and *Mathesia terticolloquiirudistarum* Maineilli. *Mathesia darderi* (Astre) is characterised by a cylindro-conical right valve and a gently domed operculiform left valve; the inner margin of the outer calcitic shell layer has scalloped and/or tubular structures; the radial bands are flat or concave; the ligamental ridge is small, in a cavity; the teeth of the left valve are approximately equally sized and longitudinally ribbed; myophores of the RV are situated on the shell wall; the myophores of the left valve are asymmetric and erect, the PM defined as a plate and the AM as a crest or a bulge (Masse and Fenerci-Masse, 2010; Fenerci-Masse et al., 2011). However, the myophores of the left valve are poorly understood because their description is based only on two longitudinal sections (Masse and Fenerci-Masse, 2010, fig. 2; Fenerci-Masse et al., 2011, fig. 7). The lack of more sections and specimens showing the myocardinal apparatus in 3D has obscured understanding of the phylogenetic relationships with other petalodontid Monopleuridae, such as *Debrunia* Masse and Fenerci-Masse and *Petalodontia* Počta. Therefore, the purpose of our taxonomic revision is to illustrate and describe the myocardinal apparatus of the left valve of *Mathesia darderi* and improve the diagnosis of the genus.

(Abbreviations: LV – left valve; RV – right valve; AT – anterior tooth; PT – posterior tooth; AM – anterior myophore; PM – posterior myophore; LR – ligamental ridge).

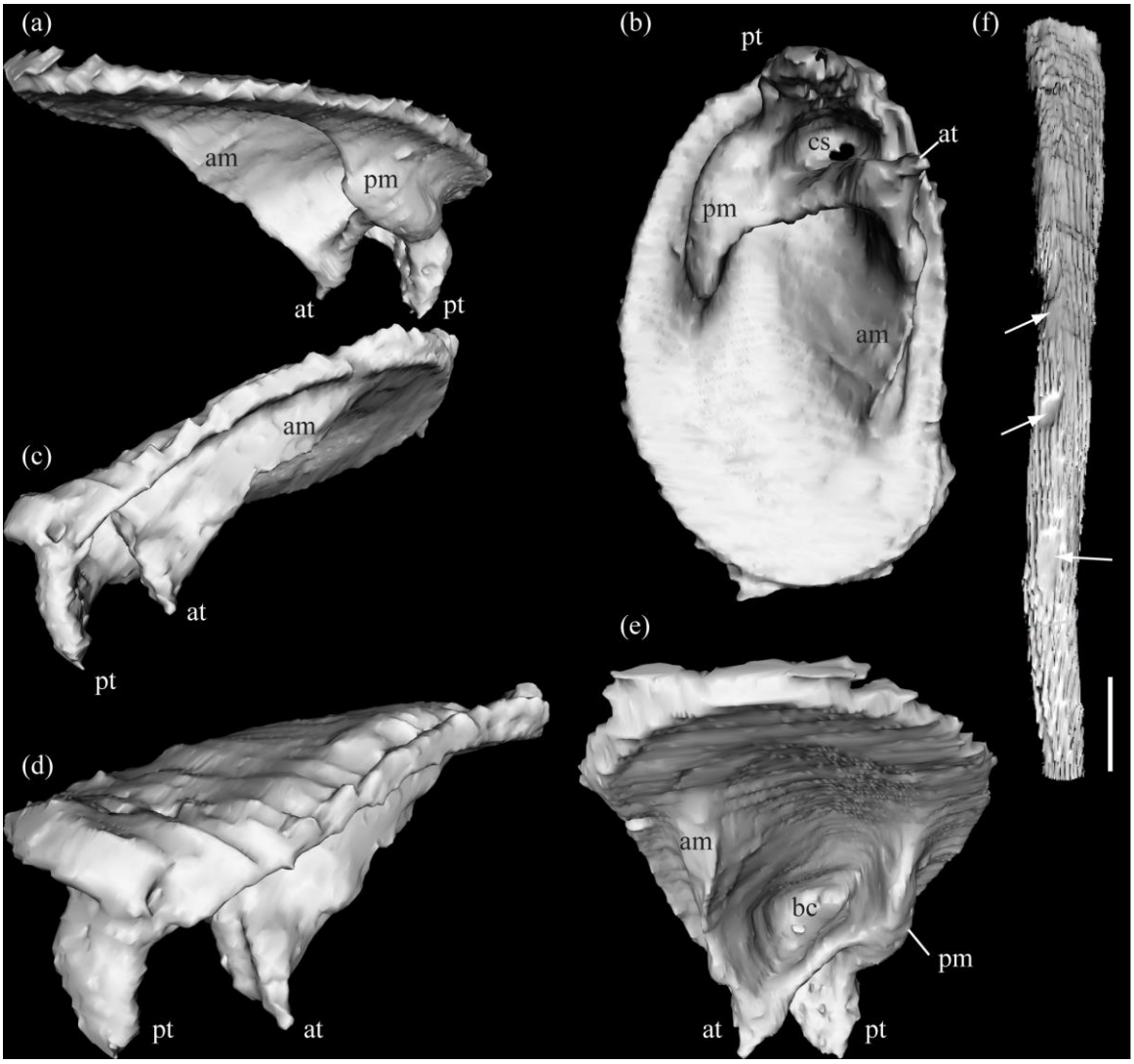

Figure 8. (a-e) Isosurfaces reconstruction of a LV of *Mathesia darderi* (scale, antero – posterior commissural diameter, 1.2 cm; dorso-ventral commissural diameters and 0.8 cm); (f) RV of *Mathesia darderi* (scale 1 cm; white arrows, zones of contact with other specimens).

ORDER: HIPPURITIDA Newell 1965
SUPERFAMILY: RADIOLITOIDEA d'Orbigny 1847
FAMILY MONOPLEURIDAE Munier-Chalmas (1873)

Genus *Mathesia* Mainelli 1996 emend. Masse and Fenerci-Masse (2010) with further revision herein.

Type species. *Mathesia tertiicolloquiirudistarum* Mainelli

Diagnosis. Cylindro-conical elongated right valve; gently convex operculiform left valve. Outer shell layer with a scalloped or tubular inner margin. The anterior myophore is an acutely wedge-shaped erect plate that is extended ventrally and is attached to the anterior tooth; the posterior myophore is also an erect plate, though inflated to give it a pediculate aspect in cross section, salient and distally rounded, and is restricted to the postero-dorsal area. The left valve teeth are erect and approximately equal. The ligamental ridge is small, in a cavity. The radial bands are flat or concave.

Mathesia darderi (Astre)
Figures 4, 8

1933 *Agria darderi* Astre, p. 103, text-figs. 1–5.
1954 *Agria darderi* var. pyrenaica Astre, plate V, figure 1, text-fig. 19.
1974 *Agriopleura darderi* (Astre), Masse and Philip, figs. 2-3.
1983 *Agriopleura darderi* (Astre), Chikhi-Aouimeur, p. 43, plate 2, fig. 6.
1992 *Agriopleura? darderi* (Astre), Masse et al., p. 206, plate 4, fig. 6.

1995 *Agriopleura*, Cestari and Sartorio, p. 95, 97, text-figs.
1996 *Mathesia tertiicolloquiirudistarum* Mainelli, p.201–209, plate 1, figs. 1–13; plate 2, figs. 1–10; figs. 4; plate 3, figs. 1–4.
1998 *Agriopleura ? darderi* (Astre), Masse et al., p. 201, figs. 10-1.
2002 *Agriopleura ? darderi* (Astre), Steuber and Bachmann, p. 736–738, text-figs. 7E, F, plate1, fig. 1.
2010 *Mathesia darderi* (Astre), Masse and Fenerci-Masse, fig. 2, p.549, fig. 4, p.550, fig. 5, p.546, fig. 6, p.551.
2010 *Mathesia darderi* (Astre), Masse et al., fig. 4, p.675
2011 *Mathesia darderi* (Astre), Fenerci-Masse et al., fig. 5, p.411, fig. 6, p.412, figs.7-8, p.413, fig.11, p.416.

Description. We ascribe to *Mathesia darderi* (Astre) a form having the following characters: the left valve is essentially slightly convex operculiform, of elliptical commissural outline with the dorso-ventral diameter larger than the antero-posterior (**Figure 8b**). Dimensions: antero-posterior commissural diameter, 8 mm; dorso-ventral commissural diameter, 12 mm; these dimensions are typical for small lower Albian specimen of *Mathesia darderi* (Fenerci-Masse et al., 2011, table 2), the ornamentation of the left valve is not described because the outer shell layer is not well preserved. The RV is cylindro-conical and the distance between the umbonal apex and mid-dorsal margin is 82 mm (**Figure 8f**). The number of longitudinal ribs decreases from the umbonal apex to the commissure, from 23 to 5. A transverse section throughout the ribs shows a darker, fine structure that is thinning inwards and connects the rib with the inner margin of the outer calcitic shell layer (**Figure 4**). The ribs are more developed on the antero-dorsal side as has been described by Masse and Fenerci-Masse (2010); the smooth surfaces without ornamentation (**Figure 8f**) are the result of contact with other specimens inside the dense lithosome. The ligamental groove is not noticeable. The inner margin of the outer shell layer of the RV presents longitudinal tubes and scalloped structures (**Figure 4**), corresponding to the type 3 microstructure of Masse and Fenerci-Masse (2010).

The LV myophores are asymmetric; the posterior myophore is a plate (**Figure 8a, b**) with an inflated distal end protruding below the commissural plane; the dorsal part of the anterior myophore is a plate attached to the anterior tooth (**Figure 8b, c, e**), its distal part is a sharp crest. The habit of this plate is triangular, its inner side inwardly inclined and its outer side orthogonal to the commissural plane; the anterior myophore is ventrally elongated but the posterior myophore is restricted to the postero-dorsal area (**Figure 8b**). The left valve teeth are approximately equal in length (**Figure 8d**); the length of the dorsal side of the PT is about 2.9 mm, the length of the dorsal side of the AT is about 2.6 mm, the anterior tooth being slightly shorter than the posterior tooth as noted by Mainelli (1996). The anterior tooth and myophore, and the posterior tooth are aligned orthogonally to the posterior myophore (**Figure 8b**).

Discussion. The myophoral organisation of the left valve of *Mathesia darderi* is similar to that of *Petalodontia*. The arrangement of their anterior myophores is identical; nevertheless, their posterior myophores are slightly different: *Mathesia* has an erect plate with an inflated end while *Petalodontia* possesses only a rounded and weakly projecting bulge (J.P. Masse and M. Fenerci-Masse, written communication, 2012). Differences may include the length of the anterior and posterior teeth: in *Mathesia darderi* the FV teeth are approximately equal whereas in *Petalodontia*, as noted by Douvillé (1900), the anterior tooth is longer. The tubular and scalloped shell microstructures that are diagnostic characters of *Mathesia* were not found in *Petalodontia* because the shell microstructures are not preserved. We only observed reminiscences of the tubular microstructure (**Figure 9**) in the inner margin of the outer calcitic shell layer of *Radiolites germari* Geinitz (1840), which Počta had included in the genus. However, this species has been taxonomically problematical because its myocardinal apparatus is not accessible and its relationship with other species of the genus *Petalodontia* stills uncertain (see discussion in Masse and Fenerci-Masse, 2009). Owing to the similarities above we suggest a close affinity of the two genera. However, it is difficult to be precise about their phyletic relationship due to the lack of information regarding the shell microstructures of *Petalodontia*.

The genus *Debrunia* Masse and Fenerci-Masse is probably the ancestor of the genus *Mathesia* due to similar organisations of the myophores (Masse and Fenerci-Masse, 2009, **Figure 8**). For a better understanding of this phylogenetic relationship further research on the forthcoming aspects may be necessary: illustration of the myocardinal apparatus of the right valve of *Mathesia*, the study of the intraspecific variability of the internal characters of *Mathesia darderi*, as well as the three-dimensional reconstruction of the myocardinal apparatus of the genus *Debrunia*.

6. CONCLUSIONS

This method of tomography based on automatic

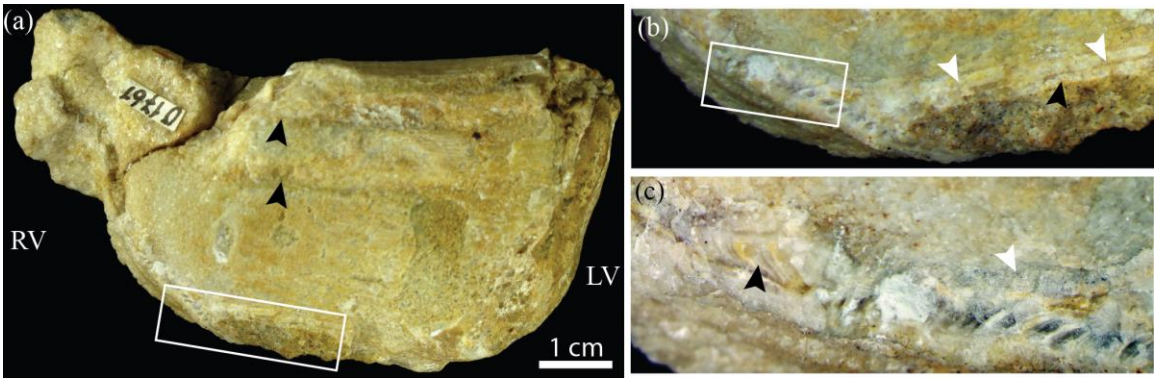

Figure 9. (a-c) *Radiolites germari* (NM-O1761): (a) anterior side of the specimen, radial bands (black arrows); (b) close up of (a) showing the inner margin of the outer calcitic shell layer (white arrow) and the growth lines of the outer calcitic shell layer (black arrow); (b) close up of (a).

grinding and serial scanning provides a maximum resolution of 2540 dpi horizontally and 10 µm vertically, which determines a voxel size of about 10 x 10 x 10 µm. The true colour tomograms are evaluated in a computer during the process. Different samples can be processed in one block with a maximum size of 15 x 15 x 30 cm^3. Moreover, the productivity varies between 5 and 39 tomograms per hour, depending on the requested quality and resolution.

The 3D-reconstructions of *Mathesia darderi* Astre offered the possibility to describe and quantify its myocardinal apparatus. The left valves myophores are asymmetric: the anterior myophore is an acutely wedge-shaped erect plate that is extended ventrally and is attached to the anterior tooth; the posterior myophore is also an erect plate, though inflated to give it a pediculate aspect in cross section, salient and distally rounded, and is restricted to the postero-dorsal area. The posterior and anterior teeth are approximately equal, with the anterior tooth being slightly smaller.

Acknowledgements. We dedicate this publication to our friend and supervisor Stefan Götz, who sadly passed away on July 30th 2012. Helpful reviews by Ann Molineux and Gavin Gunter contributed to improve this work. Constructive comments of J.P. Masse, M. Fenerci-Masse and P.W. Skelton are gratefully acknowledged. Thanks to J. Kane who kindly reviewed the English in an earlier draft of this paper. Thanks to the Paleontological department of National Museum of Prague, J. Sklenář, R. Salas, W. Stinnesbeck and M. Isenbeck-Schröter for their support and contributions. Financial support was granted by Deutsche Forschungsgemeinschaft (DFG) project (GO 1021/3-2), and by Heidelberg University ("HCE-Heidelberg Center for the Environment").

REFERENCES

Ager, D. 1965. Serial grinding techniques. In **B. Kummel and D. Raup (Eds.)**, *Handbook of paleontological techniques*, W.H. Freeman, San Francisco, 212-224.

Astre, G. 1933. Sur les petits Agria tubuleux de l'Urgo-Aptien. *Bulletin de la Société géologique de France* **5**, 99–105.

Astre, G. 1954. Radiolitidés nord pyrénéens. *Mémoire de la Société géologique de France*, **33**, 3–4, 71.

Baron-Szabo, R. C. and Fernandez-Mendiola, P. A. 1997. Cretaceous scleractinian corals from the Albian of Cabo de Ajo (Cantabria Province, N-Spain). *Paläontologische Zeitschrift*, **71**, 33-50.

Born, G. 1883. Die Plattenmodellirmethode. *Archiv für mikroskopische Anatomie*, **22**, 584-599.

Cestari, R. and Sartorio, D. 1995. *Rudists and facies of the periadriatic domain*. AGIP, S. Donato Milanese, 207.

Chikhi-Aouimeur, F. 1983. Etude paléontologique de quelques rudistes de l'Aptien supérieur du Djebel Ouenza (Algérie, NE). *Géologie Méditerranéenne*, **10**, 33–48.

Croft, W. 1950. A parallel grinding instrument for the investigation of fossils by serial sections. *Journal of Paleontology*, **24**, 693-698.

Dominguez, P., Jacobson, A. and Jefferies, R. 2002. Paired gill slits in a fossil with a calcite skeleton. *Nature*, **417**, 841-844.

Douvillé, H. 1900. Sur quelques rudistes américains. *Bulletin de la Société Géologique de France*, **28**, 205–221.

Fenerci-Masse, M., Masse, J.P., Kolodziej, B., Ivanov, M. and Idakieva, V. 2011. *Mathesia darderi* (Astre) (Bivalvia, Hippuritoidea, Monopleuridae): morphological, biogeographical and ecological changes in the Mediterranean domain during the late Barremian-Albian. *Cretaceous Research*, **32**, 407-421.

Geinitz, H. B., 1840. *Charakteristik der Schichten and Petrefacten des sächsischen Kreidegebirges. 2 Heft: A. Das Land zwischen dem Plauenschen Grunde bei Dresden und Dohna. B. Fische, Crustaceen, Mollusken*, Dresden and Leipzig, 29–62.

Götz, S. 2003. Larval settlement and ontogenetic development of *Hippuritella vasseuri* (Douvillé) (Hippuritoidea, Bivalvia). *Geologia Croatica*, **56**, 123-131.

Götz, S. 2005. *Oberkretazische Rudistenriffe beiderseits des Atlantiks - Akkumulationspotential und quantitative Paläobiologie*, 1–120. Habilitationsschrift. Fakultät für Bau, Geo- und Umweltwissenschaften der Universität Karlsruhe, Karlsruhe (thesis).

Götz, S. 2007. Inside rudist ecosystems: growth, reproduction and population dynamics. In: **R. W. Scott (Ed.)**, *Cretaceous Rudists and Carbonate Platforms: Environmental Feedback, SEPM Special Publication, Society for Sedimentary Geology*, **87**, 97–113, Tulsa, Oklahoma.

Götz, S. and Stinnesbeck, W. 2003. Reproductive cycles, larval mortality and population dynamics of a Late Cretaceous hippuritid association: a new approach to the biology of rudists based on quantitative three-dimensional analysis. *Terra Nova*, **15**, 392-397.

Hammer, Ø. 1999. Computer-aided study of growth patterns in tabulate corals, exemplified by *Catenipora heintzi* from Ringerike, Oslo Region. *Norsk Geologisk Tidsskrift*, **79**, 219-226.

Hendry, R., Rowell, A. and Stanley, J. 1963. A rapid parallel grinding machine for serial sectioning of fossils. *Palaeontology*, **6**, 145-147.

Hennhöfer, D.K., Götz, S. and Mitchell, S.F. 2012. Palaeobiology of a Biradiolites mooretownensis rudist lithosome - seasonality, reproductive cyclicity and population dynamics. *Lethaia*, **45**, 450-461.

Hughes, G., Siddiqui, S. and Sadler, R. 2004. Computerized tomography reveals Aptian rudist species and taphonomy. *Geologica Croatica*, **57**, 67-71.

Kruta, I., Landman, N., Rouget, I., Cecca, F. and Tafforeau, P. 2011. The role of ammonites in the Mesozoic marine food web revealed by jaw preservation. *Science*, **331**, 70-72.

Mainelli, M. 1996. The rudist *Mathesia tertiicolloquiirudistarum* n. gen. n. sp. in the upper Aptian of Serra Sbregavitelli, Matese, south Apennines, Italy. *Revista Mexicana de Ciencias Geologicas*, **12**, 201–210.

Masse, J.P. and Philip, J. 1974. Définition, position systématique, répartition stratigraphique et évolution du genre *Agriopleura* Kühn (Rudiste). *Géologie Méditerranéenne*, **1**, 53–62.

Masse, J.P., Arias, C. and Vilas, L. 1992. Stratigraphy and biozonation of a reference Aptian–Albian p.p. Tethyan carbonate platform succession: The Sierra del Carche Series (oriental Prebetic zone – Murcia, Spain). In: **H. A. Kollmann H. and Zapfe (Eds.)**, *New Aspects on Tethyan Cretaceous Fossil Assemblages. Österreichische Akademie der Wissenschaften, Schriftenreihe der erdwissenschaftlichen Kommissionen*, **9**, 201-222.

Masse, J.P., Arias, C. and Vilas, L. 1998. Lower Cretaceous rudist faunas of southeast Spain: an overview. Géobios, Mémoire Spécial 22, 193–210.

Masse, J.P., Beltramo, J., Martinez-Reyes, J., Arnaud-Vanneau, A., 2007. Revision of Albian polyconitid and monopleurid rudist bivalves from the New World. In: **R. W. Scott (Eds.)**, *Cretaceous rudists and carbonate platforms: environmental feedback*, SEPM special publication, **87**, 221–230, Tulsa, Oklahoma.

Masse, J.P. and Fenerci-Masse, M. 2009. *Debrunia*, a new Barremian genus of petalodontid Monopleuridae (Bivalvia, Hippuritoidea) from the Mediterranean region. *Palaeontology*, **52**, 1363–1372.

Masse, J.P. and Fenerci-Masse, M. 2010. *Mathesia* Mainelli (Hippuritoidea, Monopleuridae) from the Late Aptian−Albian of the Mediterranean Region: A Revision. *Turkish Journal of Earth Sciences*, **19**, 543-556.

Masse, J.P., Fenerci-Masse, M., Işintek, I. and Güngör, T. 2010. Albian Rudist Fauna from the Karaburun Peninsula, İzmir Region, Western Turkey, *Turkish Journal of Earth Sciences*, **19**, 671–683.

Mietchen, D., Aberhan, M., Manz, B., Hampe, O., Mohr, B., Neumann, C. and Volke, F. 2008. Three-dimensional magnetic resonance imaging of fossils across taxa. *Biogeosciences*, **5**, 25-41.

Molineux, A., Scott, R., Ketcham, R. and Maisano, J. 2007. Rudist taxonomy using X-ray computed tomography. *Palaeontologia Electronica*, **10**(6).

Molineux, A., Scott, R., Maisano, J., Ketcham, R. and Zachos, L. 2010. Blending rudists with technology; non-destructive examination of the internal and external structures of rudists using high quality scanning and digital imagery. *Turkish Journal of Earth Sciences*, **19**, 757-767.

Muir-Wood, H. 1934. On the internal structure of some Mesozoic Brachiopoda. *Philosophical Transactions of the Royal Society of London*. Series **B**, *Containing Papers of a Biological Character*, **223**, 511-567.

Olsen, F. and Whitmore Jr.F. 1944. Machine for serial sectioning of fossils. *Journal of Paleontology*, **18**, 210-215.

Ovcharenko, V. 1967. Method of studying the internal structure of fossil brachiopod shells. *Paleontology Journal*, 104-108.

Pascal, A. 1985. Les systèmes biosédimentaires urgoniens (Aptien-Albien) sur la marge Nord Ibérique. *Mémoires Géologiques de l'Úniversité de Dijon*, **10**, 1–569.

Pascual-Cebrian, E., Hennhöfer, D.K. and Götz, S. 2012. 3D morphometry of polyconitid rudist bivalves based on grinding tomography. **Facies**, doi:10.1007/s10347-012-0310-8.

Počta, F. 1889. Uber Rudisten, eine ausgestorbene Familie des Lamellibranchiaten aus der Bömischen Kreide Formation. *Rozpravy k. ceské spolecnosti nauk., V Praze*, **7**, 1-72.

Pons, J. and Vicens, E. 1988. Campanian and Maastrichtian rudists from southern Valencia Province, South east Spain. *1st International Conference on Rudists, Serbian Geological Society Special Publication* No. **2**.

Reali, S. 1992. Preliminary morphometric analysis for hippuritids taxonomy. *Geologica Romana*, **28**, 91–103.

Rosset, A., Spadola, L. and Ratib, O. 2004. OsiriX: an open-source software for navigating in

multidimensional DICOM images. *Journal of Digital Imaging*, **17**, 205-216.

Sandy, M. 1989. Preparation of serial sections. In: **R. M. Feldmann, R. E. Chapman and J. T. Hannibal (Eds.)**, *Paleotechniques. Paleontological Society Special Publication*, **4**, 143-150.

Schwarz, D., Vontobel, P., Lehmann, E.H., Meyer, C.A. and Bongartz, G. 2005. Neutron tomography of internal structures of vertebrate remains: a comparison with X-ray computed tomography. *Palaeontologia Electronica*, **8**, 30A.

Scott, R. and Weaver, M. 2010. Ontogeny and funtional morphology of a Lower Cretaceous caprinid rudist (Bivalvia, Hippuritoida). *Turkish Journal of Earth Sciences*, **19**, 527-542.

Simonpietri, G. and Philip, J. 2000. Ontogeny-phylogeny relationships in rudists: the example of Hippuritidae Gray, 1848. *Comptes Rendus de l'Academie des Sciences Series IIA Earth and Planetary Science*, **330**, 717-724.

Simpson, G. 1933. A simplified serial sectioning technique for the study of fossils. *American Museum Novitates*, **634**, 1–6.

Siveter, D.J., Sutton, M.D. and Briggs, D.E.G. 2003. An ostracode crustacean with soft parts from the Lower Silurian. *Science*, **302**, 1749.

Sollas, I. and Sollas, W. 1914. A study of the skull of a Dicynodon by means of serial sections. Philosophical *Transactions of the Royal Society of London*. Series **B**, *Containing Papers of a Biological Character*, **204**, 201-225.

Sollas, W. 1903. A method for the investigation of fossils by serial sections. *Philosophical Transactions of the Royal Society of London*. Series **B**, **196**, 214-224, 259-265.

St. Joseph, J.K.S. 1937. On *Camarototoechia borealis* (von Buch 1834, ex Schlotheim 1832). *Geological Magazine*, **74**, 33-48.

Sutton, M. 2008. Tomographic techniques for the study of exceptionally preserved fossils. *Proceedings of the Royal Society* **B**: *Biological Sciences*, **275**, 1587-1593.

Sutton, M., Briggs, D. and Siveter, D. 2001. Methodologies for the visualization and reconstruction of three-dimensional fossils from the Silurian Herefordshire Lagerstätte. *Palaeontologia Electronica*, **4**, 1-17.

Sutton, M., Briggs, D. and Siveter, D. 2005. Silurian brachiopods with soft-tissue preservation. *Nature*, **436**, 1013-1015.

Steuber, T. and Bachmann, M. 2002. Upper Aptian–Albian rudist bivalves from northern Sinai, Egypt. *Palaeontology*, **45**, 725-749.

Tafforeau, P., Boistel, R., Boller, E., Bravin, A., Brunet, M., Chaimanee, Y., Cloetens, P., Feist, M., Hoszowska, J. and Jaeger, J.J. 2006. Applications of X-ray synchrotron microtomography for non-destructive 3D studies of paleontological specimens. *Applied Physics* **A**: *Materials Science & Processing*, **83**, 195-202.

Tutton, A. 1894. An Instrument for Cutting, Grinding, and Polishing Section-Plates and Prisms of Mineral or other Crystals Accurately in the Desired Directions. *Proceedings of the Royal Society of London*, **57**, 324-330.

Vicens, E. 1994. *Estudio de la fauna de rudistas ("Hippuritidae" y" Radiolitidae") de los materiales cretácicos del Pirineo oriental: Implicaciones bioestratigráficas*, Publicacions de la Universitat Autònoma de Barcelona, Barcelona.

Walton, J. 1928. A method of preparing sections of fossil plants contained in coal balls or in other types of petrifaction. *Nature*, **122**, 571.

Watters, W.A. and Grotzinger, J.P. 2001. Digital reconstruction of calcified early metazoans, terminal Proterozoic Nama Group, Namibia. *Paleobiology*, **27**, 159-171.

Wright, F. 1915. A new crystal-grinding goniometer. *Washington Academy of Science, Journal*, **5**, 35-41.

Zdansky, O. 1938. An improved apparatus for serial sectioning of fossils. *Science*, **88**, 385.

Accepted 20th December 2012